Curve squeal in the presence of two wheel/rail contact points

G. Squicciarini[1], S. Usberti[2], D.J. Thompson[1], R. Corradi[2] and A. Barbera[2]

[1] Institute of Sound and Vibration Research, University of Southampton
University Road, Southampton SO17 1BJ, UK
E-mail: g.squicciarini@soton.ac.uk

[2] Politecnico di Milano, Dipartimento di Meccanica

Summary

A real case of a city tramcar generating very high curve squeal noise levels has motivated research in this area considering the simultaneous presence of two contact points. In this paper, available measurements are summarised in a qualitative manner in order to highlight the most important frequencies involved and a theoretical model in the frequency domain is developed with the aim of predicting curve squeal tones. Good matching is found between numerically predicted and measured unstable frequencies and a peculiar shift toward higher frequencies is found both in measurements and predictions.

1 Introduction

Curve squeal is one of the most serious noise problems connected with the operation of trains, tramways and metros in urban environments. The phenomenon has been analysed by many authors, by means of both experimental tests and theoretical models, and it is agreed that it is produced by the self-excited vibration of the wheel, as a result of the contact phenomena taking place at wheel-rail interface during curve negotiation.

Although some research has been carried out in order to point out the influence of the different contact conditions at the inner and outer wheel of a leading axle on the occurrence of squeal noise, no specific investigation for urban tramways with grooved rails is available. This paper describes research into squeal noise measurements and modelling for a case of a city tramway with independent resilient wheels on very sharp curves [1]. Very high squeal noise levels were recorded and both the flange back of the inner wheel and the flange of the outer wheel were believed to be in contact with the head and grooved-head due to the highly worn condition of the rail.

Since Rudd's paper [2], there has been a general understanding that flange contact does not represent an important source of noise in curves and in [3][3] it was even shown that squeal noise was not occurring with the contact point located on the flange while it appeared as soon as the wheel was slightly moved to have

the contact point on the tread. However, it is known that squeal noise can be also generated by flange contact (see e.g. [4][4]) involving predominantly radial modes of the wheel. Indeed, measurements described in [1] represent exactly this situation and give an important motivation for investigating the effect that two contact points have on squeal noise.

To the authors' knowledge there are no models available in the literature to address curve squeal in the presence of two-point contact; therefore Sect. 3 is devoted to describing how the model developed by Huang [5][5] has been extended and updated to consider the simultaneous presence of two contact points. It is known that the curve squeal phenomenon is far from being deterministic and parameters like temperature, humidity and even dirt and particles on the rail can have a strong effect on its occurrence. For this reason, in the model presented here, some input parameters are defined as uncertain variables. As a result, the model is used to give the frequency values of possible unstable eigenvalues of the system while the range of uncertain parameters is randomly spanned. The definition of the nominal kinematic condition at the contact (position of the contact points and creepages) has been determined by means of a vehicle dynamics numerical model described in [6][6]. The model developed is of general purpose and can be used for any wheel-rail combination; as a first application results have been verified against measurements of [1][1] showing a good reliability in predicting the frequencies involved in curve squeal.

2 Measurements

Experimental data was collected in a test campaign on a curve which particularly suffers from squeal noise problems. The selected test section is an 18 m radius, left curve, with grooved rails and ballasted track. The test vehicle is a modern articulated city tram, with seven car-bodies and four bogies, equipped with resilient and independently rotating wheels.

Before performing test runs on the selected curve, experimental modal analysis was carried out on the test wheel mounted in the bogie through its own bearings and in suspended configuration. The main wheel vibration modes falling in the frequency range involved in the squeal noise (up to 4 kHz) were identified in terms of natural frequencies, mode shapes and damping ratios. Those that will appear to be involved in squeal are identified in Fig. 1.

In a second stage an axisymmetric Finite Element model of the resilient wheel has been developed; rubber parameters have been tuned to match identified modes. Identified damping ratios have been used along with numerically computed mode shapes and natural frequencies to prepare a modal model of the wheel. This is one of the inputs required for the curve squeal model. Mobilities obtained numerically are compared with measurements in Fig. 1 showing a good agreement in the range of interest.

Line tests on the selected curve were then performed, in two different configurations. The instrumented wheel first was positioned on the leading axle of

the second bogie, on the outer side of the curve. Then it was moved to the inner side of the same axle, and the train passages on the test curve were repeated. Since, in these two cases, the wheel experiences completely different contact conditions, their influence on the excitation of the squeal can be clearly identified. During each passage of the test tram, simultaneous measurements of wheel vibration, rail vibration and radiated noise were taken [1].

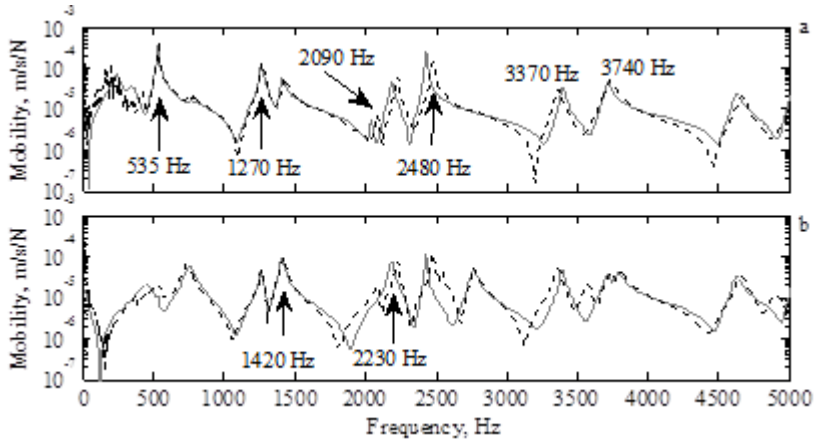

Fig. 1. Wheel mobilities at nominal contact point. a: axial direction. b: radial direction. – – –: measurements; ——: FE model.

To summarise the wheel behaviour in terms of squeal noise the inner wheel of the leading axle is taken as example; in this case the flange back is in contact with the grooved head. Fig. 2 shows the spectrogram of the wheel vibration velocity in radial and axial directions during the passage through the curve. Although the darker corridors in the figure are relatively wide it is still possible to identify the following as the frequencies mainly involved in squeal: 530 Hz, 1330 Hz, 1550 Hz, 2100 Hz, 2550 Hz, 3600 Hz and 3730 Hz. The contribution at 3100 Hz is likely to be the second harmonic of 1550 Hz which appears due to the non-linearity of the phenomenon.

According to curve squeal theory each tone recorded during the vehicle passage is expected to be related to a wheel mode. In this case this is not always straightforward. In fact, it is peculiar to observe that the modes at 1270 Hz and 1420 Hz seem to generate squeal at higher frequencies (1330 Hz and 1550 Hz) and the mode at 2480 Hz has a similar behaviour.

3 Theoretical model

The model consists of a linear description of the wheel and rail dynamics while the non-linear representation of friction coefficients as a function of creepages presented by Kraft [7][7] is adopted to calculate the contact forces. A stability

analysis of the open loop transfer function of the overall system yields the possible unstable frequencies.

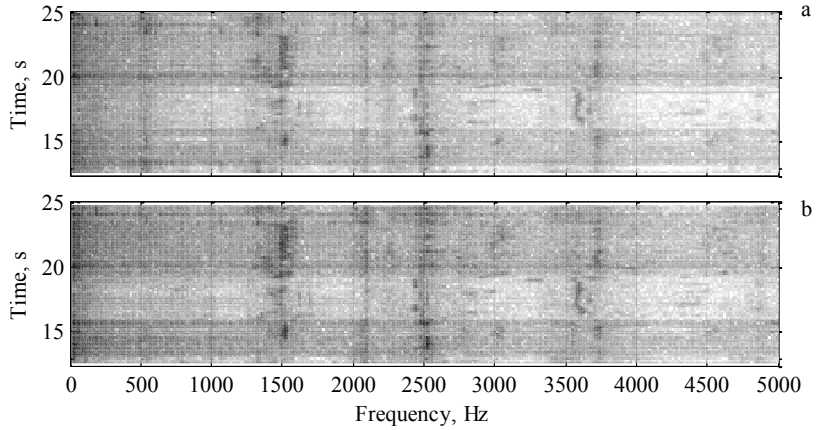

Fig. 2. Spectrogram of inner wheel vibration velocity during tram pass-by. a: axial; b: radial. Darker regions correspond to higher levels.

Fig. 3a shows the general structure of the model. The wheel is represented by means of its modal basis to give the mobilities at the nominal contact point. By knowing the steady state position of the contact points along the curve, direct and transfer mobilities at these locations are calculated by means of rigid translations and rotations. $Y^{W}_{ij,kl}$ in the figure represents a single element of the wheel mobility matrix, subscripts *i* and *j* represent the degrees of freedom (*d.o.f.*) at the contact while *k* and *l* represent the contact points (see Fig. 3b). The *d.o.f.* considered in the model are longitudinal, lateral, normal to contact plane and spin (rotation around the normal); it is believed that the other two rotations can be neglected.

For the track, different analytical models are used depending on the *d.o.f.* considered. For the vertical direction a Timoshenko beam on a double elastic layer is adopted while a multi-beam model described in [8] allows lateral vibrations to be coupled with torsion. Simple formulae are implemented to estimate longitudinal and spin mobilities. Again, track mobilities are transferred to the contact points by means of rigid rotations and translations. $Y^{R}_{ij,kl}$ in the figure represents one element of the rail mobility matrix.

The contact stiffness is considered in the vertical direction for the wheel-rail contact mobility matrix ($Y^{C}_{ij,kl}$) and is calculated according to Hertz theory.

Complex dynamic sliding velocities $\mathbf{V}^s$ and complex dynamic contact forces $\mathbf{F}$ at the contact points are finally related through mobility matrices as follows:

$$\mathbf{V}^s = \begin{Bmatrix} \mathbf{V}_1^s \\ \mathbf{V}_2^s \end{Bmatrix} = \begin{bmatrix} \mathbf{Y}_{11} & \mathbf{Y}_{12} \\ \mathbf{Y}_{12} & \mathbf{Y}_{22} \end{bmatrix} \begin{Bmatrix} \mathbf{F}_1 \\ \mathbf{F}_2 \end{Bmatrix} = \mathbf{YF} \tag{3.1}$$

where each element of the matrix **Y** is calculated by adding wheel, rail and contact mobilities and the subscripts in eq. (3.1) indicate the two contact points.

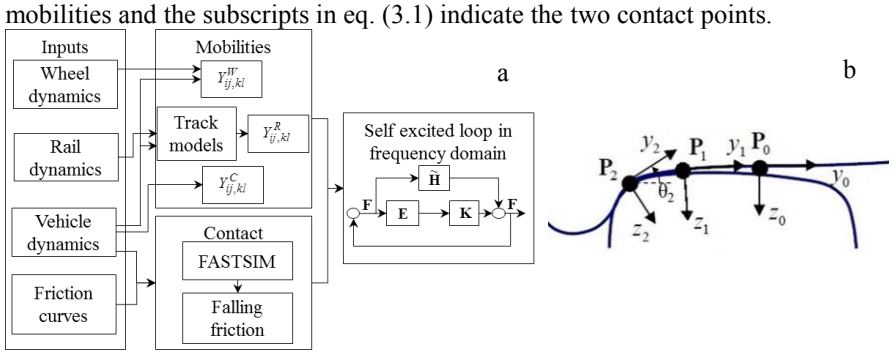

Fig. 3. a: general structure of the model. b: reference frames at contact points 1 and 2 (0 is nominal contact point).

After algebraic manipulation taking into account that the vertical sliding velocity is zero, the following quantities can be defined:

$$\mathbf{d}_n^T = \left\{ Y_{13,1n} \quad Y_{23,1n} \quad Y_{63,1n} \quad Y_{13,2n} \quad Y_{23,2n} \quad Y_{63,2n} \right\} \qquad n = 1,2 \tag{3.2}$$

$$\mathbf{a}_n^T = \left\{ \frac{Y_{31,n1}}{Y_{33,nn}} \quad \frac{Y_{32,n1}}{Y_{33,nn}} \quad \frac{Y_{36,n1}}{Y_{33,nn}} \quad \frac{Y_{31,n2}}{Y_{33,nn}} \quad \frac{Y_{32,n2}}{Y_{33,nn}} \quad \frac{Y_{36,n2}}{Y_{33,nn}} \right\} \; n = 1,2 \tag{3.3}$$

$$\mathbf{b}_n^T = \frac{Y_{33,11}Y_{33,22}}{Y_{33,11}Y_{33,22} - Y_{33,12}^2} \left(-\mathbf{a}_n^T + \frac{Y_{33,12}}{Y_{33,nn}} \mathbf{a}_{3-n}^T \right) \; n = 1,2 \tag{3.4}$$

and eq. (3.1) rewritten as

$$\mathbf{V}^s = \left(\mathbf{C} + \mathbf{d}_1 \mathbf{b}_1^T + \mathbf{d}_2 \mathbf{b}_2^T \right) \mathbf{F} = \mathbf{E}\mathbf{F} \tag{3.5}$$

The matrix **C** in eq. (3.5) is formed from the matrix **Y** by removing the rows and columns related to the vertical direction; vectors **d** and **b** are defined in eq. (3.2)-(3.4). **E** is one of the key elements of the self-excited loop represented in Fig. 3a.

To describe the relationship between friction coefficients and creepages the FASTSIM algorithm is adopted (see [9][9]). To introduce the falling region, a heuristic correction formula (see [7][5, 7]) of the form:

$$\tau_k = \left(1 - \lambda_k e^{-\kappa_k / \gamma_{tot}} \right) \tag{3.6}$$

is assumed; λ_k and κ_k are empirically determined for each contact point k and γ_{tot} combines the contribution of all creepages.

At a contact point k the linearized relation between contact forces and creepages can be expressed, independently of the other contact point, as:

$$\mathbf{F}_k = \mathbf{K}_k \mathbf{V}_k + \mathbf{H}_k \mathbf{F}_{3,k} \tag{3.7}$$

where elements of matrix $\mathbf{K}_k$ and vector $\mathbf{H}_k$ are defined as

$$K_{ij,k} = \frac{N_{0,k}}{V_0} \frac{\partial \mu_{i,k}}{\partial \gamma_{j,k}}; \qquad H_{i,k} = \mu_{i,k} + N_{0,k} \frac{\partial \mu_{i,k}}{\partial f_{3,k}} \tag{3.8}$$

In eq. (3.8) $N_{0,k}$ is the normal force at point k, $\mu_{i,k}$ is the friction coefficient in direction i at contact point k, $\gamma_{i,k}$ is the creepage in direction i at contact point k and $f_{3,k}$ is the dynamic force in the direction normal to the contact plane at point k.

Combining eq. (3.7) and (3.4) with (3.5) the equation for the self-excited loop of Fig. 3a results as

$$\mathbf{F} = \mathbf{KEF} + \mathbf{H}\begin{Bmatrix}\mathbf{b}_1^T \\ \mathbf{b}_2^T\end{Bmatrix}\mathbf{F} = \mathbf{KEF} + \tilde{\mathbf{H}}\mathbf{F} \tag{3.9}$$

In order to find the possible unstable frequencies, the eigenvalues of the open loop transfer function are computed and those having an imaginary part equal to zero and a real part greater than unity are classified as possible sources of instability.

4 Results

The theoretical model described in Sect. 3 has been verified against measurements summarised in Sect. 2. In order to obtain reliable values for the vehicle dynamic parameters a multi-body model of the tram has been developed by means of the software described in [6]. Steady state creepages and contact point positions have been obtained. Where necessary, variability is added to these parameters. The most important uncertain and deterministic input parameters are summarised in Tab. 1.

Table 1. Input parameters at contact points 1 and 2 for inner and outer wheels. *U* indicates a uniform distribution between the stated limits.

Name	Unit	Description	Values	
			Inner	Outer
$N_{0,1}$	kN	Normal force 1	U(17,25)	U(14.5,21.7)
$N_{0,2}$	kN	Normal force 2	U(0,6.5)	U(0,12)
V_0	m/s	Speed	U(1.9,3.6)	U(1.9,3.6)
κ_1	-	Eq. (3.6) 1	U(0.04,0.06)	U(0.04,0.06)
κ_2	-	Eq. (3.6) 2	U(0.12,0.17)	U(0.12,0.17)
λ_1	-	Eq. (3.6) 1	0.8	0.8
λ_2	-	Eq. (3.6) 2	0.8	0.8
θ_1	°	Contact angle 1	U(2.4,3.4)	U(-3.4,-2.4)
θ_2	°	Contact angle 2	U(-73,-63)	U(-76,-66)
γ_{x1}	-	Creepage x 1	U(0.0038,0.0057)	U(0.0067,0.0101)
γ_{y1}	-	Creepage y 1	U(-0.0651,-0.0434)	U(-0.0651,-0.0434)
γ_{sz1}	1/m	Spin-creep z 1	U(0.12,0.18)	U(0.12,0.18)
γ_{x2}	-	Creepage x 2	U(-0.0310,-0.0207)	U(-0.0193,-0.0128)
γ_{y2}	-	Creepage y 2	U(-0.1587,-0.1058)	U(-0.2000,-0.1334)
γ_{sz2}	1/m	Spin-creep z 2	U(2.2560,3.3840)	U(2.2960,3.4440)
$\mathbf{P}_1$	mm	Contact 1	[0 U(-9.5,0.5) -0.22]	[0 U(-9,1) 0.2]
$\mathbf{P}_2$	mm	Contact 2	[50.1 40.2 10.4]	[50.6 -20 8]

In order to produce a single set of inputs and to run a single case, uncertain parameters are randomly extracted from a uniform distribution and, for each case, the eigenvalues of the open loop transfer function are calculated as a function of frequency. Fig. 4 summarises the results for the inner and outer leading wheels, with black dots depicting the unstable frequencies for each run; the wheel mobility at the flange contact point is also shown for reference. A total of 450 cases have been calculated giving an idea of the variability of the phenomenon.

The model predicts unstable frequencies that are very close to measured ones (Fig. 2). In particular the most important frequencies 1330 Hz, 1550 Hz and 2550 Hz are the most likely to be unstable in the model as well. Frequencies such as 2100 Hz and 3700 Hz that, although present in the measurements, have less importance in terms of levels and persistency, are also found in the predictions.

Interestingly, in the predictions it is often found that unstable eigenvalues have higher frequencies than the corresponding natural mode. For example, the mode at 1420 Hz appears to generate squeal at around 1550 Hz. This has been verified by adding fictitious damping to the mode at 1420 Hz; as a consequence the unstable frequencies at around 1550 Hz disappeared. Further research is in progress to understand better the details of the phenomenon. In this sense it has been verified that neither the high damping values related to the resilient wheel nor the presence of the rail in the model are responsible. Moreover it has also been determined experimentally that the positions of the peaks in the wheel FRF are hardly influenced by the vehicle load; therefore this also cannot explain the shift in frequency.

Finally, by modifying damping ratios in the wheel modal model, those values capable of decreasing the chances of instability can be sought. In this case, multiplying the damping ratios of the modes at 2480 Hz, 1420 Hz and 1270 Hz by factors of 15, 5 and 6, respectively, would greatly decrease the occurrence of squeal. By repeating the same analysis that generated Fig. 4 it has been found that, with this amount of added damping, these modes are likely to be involved in squeal in less than 10% of the 450 cases considered.

5 Conclusions

Despite the relatively low interest in the railway noise literature, curve squeal can also occur due to flange contact; moreover, when a grooved rail or a check rail is fitted onto the track, the flange-back contact can also have a significant role.

A real case of a tramcar negotiating a sharp curve has given the motivation for developing a model capable of considering two-point contact. By performing stability analysis of the open loop transfer function, possible unstable frequencies have been predicted. A degree of uncertainty has been given to the most important input parameters.

Qualitative comparison with measurements showed that the most important tones recorded during the tram pass-by can be found in the predictions. Noticeably, the same frequency shift between wheel natural frequency and

unstable frequency value as measured is found in the predictions. Further investigations are in progress to understand the physical reason for this.

In order to verify whether all the predicted unstable frequencies would really appear and what the noise levels would be, a time domain solution of the same loop can be developed.

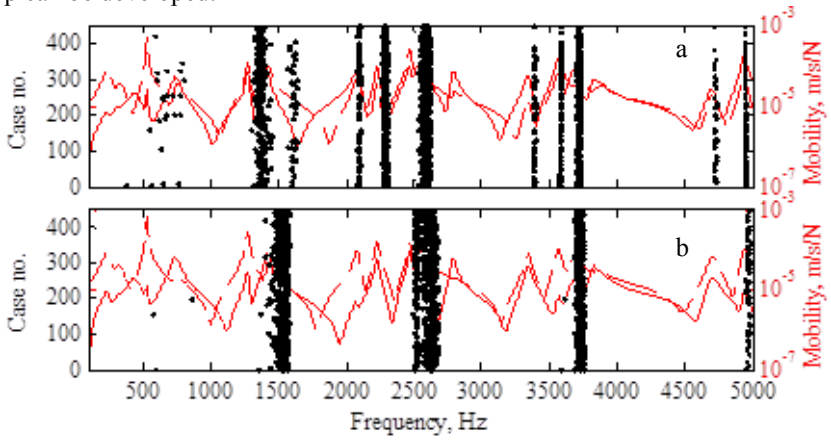

Fig. 4. Black dots: curve squeal occurrences. Lines: mobility at flange contact point. – – –: normal; ——: tangent. a: inner wheel. b: outer wheel.

References

[1] Corradi, R., et. al., Experimental investigation on squeal noise in tramway sharp curves, Proc. EURODYN 2011, Leuven; Belgium.

[2] Rudd, M. J., Wheel/rail noise—Part II: Wheel squeal, Journal of Sound and Vibration, vol. 46, no. 3, 381-394 (1976).

[3] Chiello, O., et. al., Curve squeal of urban rolling stock—Part 3: Theoretical model, Journal of Sound and Vibration, vol. 293, no. 3-5, 710-727 (2006).

[4] Monk-Steel, A. D., et al., An investigation into the influence of longitudinal creepage on railway squeal noise due to lateral creepage, Journal of Sound and Vibration, vol. 293, no. 3-5, 766-776 (2006).

[5] Huang, Z., Theoretical Modelling of Railway Curve Squeal, PhD Thesis, University of Southampton, Institute of Sound and Vibration Research, 2007

[6] Cheli, F., Corradi, R., Facchinetti, A., A numerical model to analyse the dynamic behaviour of modern tramcars, 2002, Proc. Mini Conf. on Vehicle System Dynamics, Identification and Anomalies, pp. 183-190

[7] Kraft, K., 'Der Einfluß der Fahrgeschwindigkeit auf den Haftwert zwischen Rad und Schiene', AET 22 addendum to ETR, pp. 58-78 (1967).

[8] Wu, T.X., Thompson, D.J., Analysis of lateral vibration behavior of railway track at high frequencies using a continuously supported multiple beam model, J. Acoust. Soc. Am., vol. 106, no. 3, 1369-1376 (1999).

[9] Kalker, J.J., A Fast Algorithm for the Simplified Theory of Rolling Contact, Vehicle System Dynamics, vol. 11, no. 1, 1-13 (1982).